L-subshell ionization of Ce, Nd, and Lu by 4–10-MeV C ions

G. Lapicki,[1,*] A. C. Mandal,[2] S. Santra,[3] D. Mitra,[3] M. Sarkar,[3] D. Bhattacharya,[3] P. Sen,[3] L. Sarkadi,[4] and D. Trautmann[5]
[1]*Department of Physics, East Carolina University, Greenville, North Carolina 27858, USA*
[2]*Department of Physics, University of Burdwan, Burdwan 713104, India*
[3]*Saha Institute of Nuclear Physics, 1/AF Bidhannagar, Kolkata 700064, India*
[4]*Institute of Nuclear Research of the Hungarian Academy of Sciences (ATOMKI) H-4001, Debrecen, Pf. 51, Hungary*
[5]*Institute für Theoretische Physik, Universität Basel, Klingelbergstrasse 82, CH-4056 Basel, Switzerland*
(Received 29 December 2004; published 30 August 2005)

$Ll, L\alpha, L\beta, L\gamma, L\gamma_{1+5}, L\gamma_{2+3}, L\gamma_{4+4'}$ x-ray production cross sections of $_{58}$Ce, $_{60}$Nd and $_{71}$Lu induced by 4-, 6-, 8-, and 10-MeV carbon ions were measured. For Lu, $L\gamma_{2+3}$ is separated from $L\gamma_{2+3+6}$ after revision of the technique of Datz *et al.* so that $L\gamma_{1+5}$ was used instead of $L\gamma_1$, the $L\gamma_{4+4'}/L\gamma_{1+5}$ ratio was corrected for multiple ionization, and uncertainties in $L\gamma_{4+4'}$ were incorporated in the fitting process. *L*-subshell ionization cross sections were extracted as a weighted average from two combinations of these cross sections, $\{L\alpha, L\gamma_{1+5}, L\gamma_{2+3}\}$ and $\{L\alpha, L\gamma_{1+5}, L\gamma\}$. It is shown that, to within a few percent, the first of these two combinations results in the identical cross sections as this weighted average. Within 10%, permutations of different sets of single-hole atomic parameters yielded the same ionization cross sections. These cross sections are typically within 15% and at most 35% of the cross sections obtained with atomic parameters that were altered in two different ways for multiple ionization. Extracted subshell and total *L*-shell ionization cross sections as well as Ce and Nd data of Braziewicz *et al.* are compared with the ECPSSR theory of Brandt and Lapicki that accounts for the energy-loss (E), Coulomb-deflection (C), perturbed-stationary-state (PSS) and relativistic (R) effects. These measurements are also compared with the ECPSSR theory after its corrections—in a separated and united atom (USA) treatment, and for the intrashell (IS) transitions with the factors of Sarkadi and Mukoyama normalized to match *L*-shell cross section with the sum of *L*-subshell cross sections—as well as with the similarly improved semiclassical approximation of Trautmann. For Ce and Nd, the agreement of the extracted ionization cross sections with these theories is poor for L_1 and good for L_2, L_3, and total *L* shell ionization. For the L_2 subshell, this agreement is better for Ce and Nd than for Lu. The ECPSSR theory corrected for the USA and IS effects is surprisingly good for the L_1-subshell ionization of Lu, while at 4 MeV a similarly corrected semiclassical approximation is in excellent agreement with L_2 and L_3 data but overestimates the L_1 measurement by almost a factor of 2.

DOI: 10.1103/PhysRevA.72.022729 PACS number(s): 34.50.Fa

I. INTRODUCTION

Atomic inner-shell ionization studies have progressed over the last four decades, resulting in close and stringent comparisons of the measured x-ray production spectra with the predictions of theoretical models. As a consequence, there is now a large body of data on particle-induced x-ray cross sections. A quick survey of x-ray cross-section data would reveal that their large portion is on *K* and *L* shells ionized by protons and α particles [1–4]. X-ray production cross sections by heavy ions, however, are comparatively scanty, particularly so for *L*-subshell ionization.

At the time when advances were being made in the experimental studies of inner-shell ionization, several theories such as the plane-wave Born approximation (PWBA) [5], the binary encounter approximation (BEA) [6], the semiclassical approximation (SCA) [7] for direct ionization of inner shells, and the Oppenheimer-Brinkman-Kramers formulas of Nikolaev (OBKN) [8] for electron capture were superceded by ionization theories that go beyond the first-order Born perturbation theory. In the ECPSSR theory for direction ionization [9], this was done in the perturbed-stationary-state (PSS) approach with analytical functions accounting for the projectile energy loss (E), Coulomb deflection (C), and relativistic (R) motion of the inner shell electron—the effects that are not included in the standard PWBA [5]. Similar functions were applied to go beyond the OBKN for electron capture [10]. The E, C, and R effects were also included in the SCA of Trautmann *et al.* [11] with exact limits for momentum transfers, the hyperbolic trajectory for the projectile, and Dirac Hartee-Slater wave functions for the target electron The PSS effect was partially simulated in the SCA in the united atom (UA) limit in treatment of the target [11]. Both the ECPSSR [9,10] and the SCA [11] were recently further modified in a united and separated atom (USA) manner as done, respectively, in Refs. [12] and [13]. After a replacement of the PSS treatment with the USA approach in the ECPSSR theory, we will refer to it as the ECUSAR theory. The SCA theory of Trautmann *et al.*, modified as in Ref. [13] for the USA effect, will be denoted with the CUSCAR acronym to emphasize that beyond the original straight-line and nonrelativistic SCA [7]. The CUSCAR theory accounts for the Coulomb deflection, a united and separated simulation of the binding effect, and uses relativistic wave functions for inner shells.

*Electronic address: lapicki@physicist.net

It is known that for low-Z_1 projectiles like H or He, the ECPSSR theory is quite successful in describing the experimental trends [14]. For heavy-ion projectiles, however, the disagreement between the measurements and theory for L-subshell ionization often reaches an order of magnitude especially at low projectile energies. This indicates that the theoretical treatment of the ion-atom collision process within the ECPSSR and the SCA of Trautmann *et al.* requires further modification. Sarkadi and Mukoyama [15] were first to suggest that the mechanism of vacancy sharing among the subshells—intrashell (IS) effect—might be the cause of disagreement. By treating the ionization and subshell coupling as two successive steps of the same collision process, Sarkadi and Mukoyama initially introduced a classical two-step model to account for this IS effect [15]. Subsequently, this model was developed into a full quantum mechanical treatment of the IS effect [16–20].

We are mainly interested in finding out the extent to which the introduction of the IS coupling bridges the gap between the measured values and the theoretical predictions. In earlier investigations on the L-subshell ionization of heavy elements of $_{79}$Au and $_{83}$Bi [21–23], we found that inclusion of the IS effect did, indeed, substantially improved the agreement between measurements and theory for the L_2 subshell, worsen it for the L_1 subshell, and made no essential difference for the L_3 subshell [22]. The present work is an extension of these studies to $58 \leqslant Z_2 \leqslant 71$ targets to assess if the IS effect is valid in the Z_2 range of such target elements. We will also revisit in Sec. IV our earlier conclusions about the IS effect for gold L-subshell ionization [22] in light of a later development which imposed the requirement that the total L-shell ionization cross section calculated with the IS factors be identical to the cross section evaluated without these factors [13].

Extraction of cross sections for L-subshell ionization of $_{58}$Ce, $_{60}$Nd, and $_{71}$Lu targets by 4–10-MeV carbon ions from the measured x-ray production of $L\alpha$, $L\beta$, and $L\gamma$ series requires a considerable number of atomic parameters (i.e., branching ratios and atomic yields). Use of different sets of single-hole atomic parameters may give rise to a spread in the extracted ionization cross sections. After an enumeration of experimental details in Sec. II, this aspect plus the critical issue of multiple ionization and its effect on the atomic parameters are addressed in Sec. III. In Sec. IV, the extracted L-subshell ionization cross sections are compared to the predictions of the ECPSSR and its modification for the USA and IS effects as well as the CUSCAR theory modified for the IS effect. Section V concludes with a list of our main findings.

II. EXPERIMENTAL DETAILS

Details of the experimental arrangement were described in our earlier work [21]; thus only a short description is given here. The experiment was performed with the 3-MV 9SDH-2 Tandem Pelletron at the Institute of Physics, Bhubaneswar, India. Ions of C^{2+} (at 4 and 6 MeV) and C^{3+} (at 8 and 10 MeV) were used for this measurement. The beam passed through two graphite collimators of 3 mm in diameter located at a distance of 75 mm from each other so that the beam spot on the target, placed at 60° with respect to the beam, was approximately 3 mm. A Si(Li) detector having a resolution of 160 eV at 5.9 keV was located at 105° to the beam, and simultaneous measurement of the back scattered projectile was done with a Si surface barrier detector kept at an angle 135° to the beam. The target thicknesses were 110 μg/cm^2 Ce on carbon backing, 13.0 μg/cm^2 Nd on aluminum backing, and two 5.6- and 16.5-μg/cm^2 Lu targets also on aluminum backing. The target and particle detector were housed in a scattering chamber that was kept at a vacuum of 10^{-6} Torr by a turbo molecular pump. The spectra of the x rays and of the backscattered projectiles were collected simultaneously on separate analog-to-digital converters (ADC's) so that the x-ray production cross section could be determined independently of variations in the target thickness and fluctuations, if any, in the beam current. The average beam current was ~10 nA, and the time for a particular run was typically 2 h. The total count rate was always kept under 1000 counts/s.

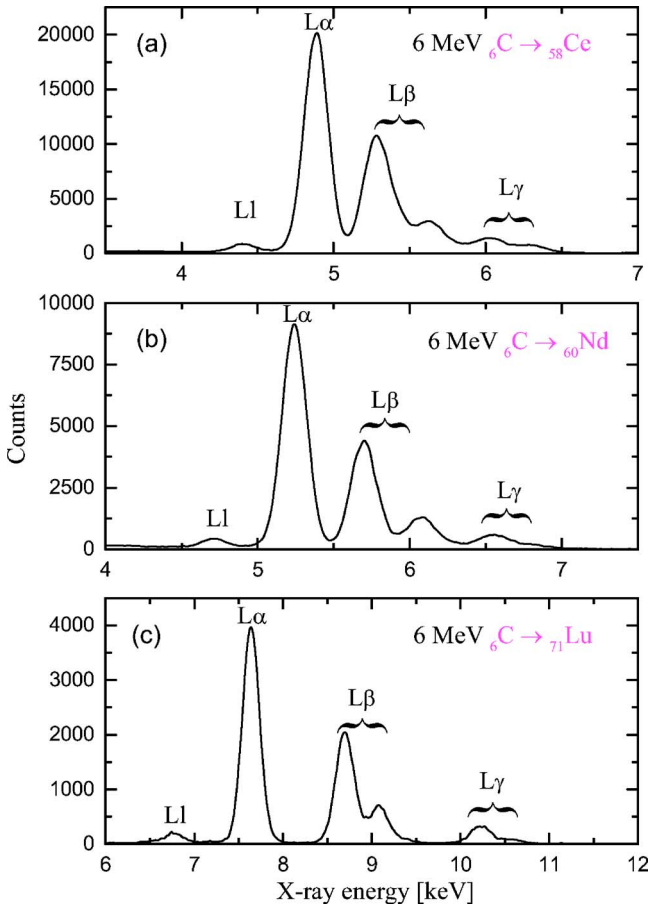

FIG. 1. (Color online) Typical L x-ray spectra of cerium, neodymium, and lutetium induced by 6-MeV carbon ions.

III. DATA ANALYSIS

Typical L x-ray spectra of Ce, Nd, and Lu bombarded with 6-MeV C^{2+} ions are shown in Fig. 1. The spectra were analyzed with a nonlinear least-squares fitting method using the program ACTIVE [24] by assuming a Guassian line shape

for the full energy x-ray peaks and a polynomial background. The x-ray production cross sections for the L lines were determined from the relation

$$\sigma_p = \frac{\sigma^R(\theta)(d\Omega)N_x}{\varepsilon N}F, \tag{1}$$

where σ_p is the x-ray production cross section for the x-ray peak Lp $(Ll, L\alpha, L\beta, \ldots)$; $\sigma^R(\theta)$ is the Rutherford scattering cross section at an angle 135° (for the present measurement), corrected for screening according to Huttel *et al.* [25], $(d\Omega)$ is the solid angle subtended by the particle detector at the target, which was 0.00173 in the present case, and N_x is the peak integral of the x-ray line. With the peaks due to the elastic scattering from the target and its backing material well separated, N is the number of the projectiles that scatter elastically from the target element. F is the correction factor due to slowing down of the projectiles in the target of finite thickness, which includes corrections due to self absorption of the x rays in the target; ε is the effective efficiency of the Si(Li) detector including solid angle.

The slowing-down factor F was calculated following the method of Papp *et al.* [26]. The x-ray self-absorption factor was calculated taking the path of the x rays inside the target as half of the target thickness and using the total absorption coefficient values from the XCOM [27].

The effective efficiency (intrinsic efficiency including the geometrical factor) of the Si(Li) detector in the energy range of 4–12 keV was carefully measured in the same geometry as was used in the actual measurement. Thin targets of Ca, V, Cr, Fe, Ni, and Ge bombarded by 3-MeV protons produced the necessary K x rays. The backscattered protons were collected simultaneously. The K-shell "reference" ionization cross sections from the compilation of Paul and Sacher [2], the fluorescence yields from Hubbell *et al.* [28], and the $K\alpha/K\beta$ values from Salem *et al.* [29] were used to get the K x-ray yields. The efficiency values obtained in this manner and a three-free-parameter curve fitted to them to within 5% are shown in Fig. 2.

It has been known [30–32] that particle-induced x rays originating from the states with $j \geq 3/2$ are anisotropic. In the present work, only the $L\alpha$ and $L\gamma$ lines will be used for the extraction of subshell ionization cross sections. $L\gamma$ lines originate from the states with $j=\frac{1}{2}$, and so their cross sections are totally isotropic. $L\alpha$ x rays are practically isotropic because its $L\alpha_1$ and $L\alpha_2$ components have opposite anisotropy. It has been mentioned [21] that in our energy range, the intensity of the carbon induced $L\alpha$ lines from Au deviates from the isotropic distribution by only 1%. Thus, for the extraction of subshell ionization cross sections, the relevant x rays are assumed to be isotropic.

The major uncertainties in the present x-ray production cross section measurement stem from (1) a 7% error in the detector efficiency, (2) a 5% error in the correction factor F, (3) a less than 1% error in the backscattered yields, and (4) a 1%–10% statistical error arising from the x-ray yields except for the $L\gamma_{4+4'}$ peak where such error rises to 55% at 4 MeV. The average errors over all targets and projectile energies in Ll, $L\alpha$, $L\beta$, $L\gamma$, and $L\gamma_{1+5}$ are 10%, and in a tiny $L\gamma_{4+4'}$

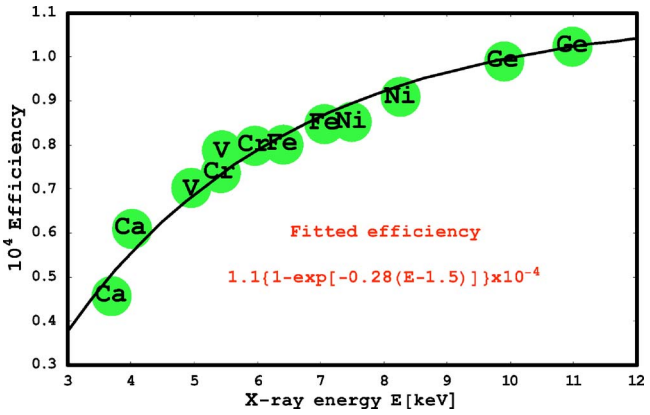

FIG. 2. (Color online) Efficiency of the Si(Li) detector determined from the measured $K\alpha$ and $K\beta$ x-ray production cross sections for the labeled elements normalized to a fit for empirical cross sections [2] partitioned into $K\alpha$ and $K\beta$ using $K\alpha/K\beta$ ratios [29]. To within 5%, the curve is a three-parameter fit to the efficiency points which are drawn with the circle of uncertainty for this determination.

almost 40%. $L\gamma_{2+3}$ has errors of 10% for Ce and 12% for Nd. For Lu, errors in $L\gamma_{2+3}$ are 26% when isolated from $L\gamma_{2+3+6}$ by the standard Datz technique [33] and 36% after this technique is modified for multiple ionization. The x-ray production cross sections for these peaks are listed in Table I for different projectile energies.

The measured x-ray production cross sections for the most commonly resolved Ll, $L\alpha$, $L\beta$, and $L\gamma$ peaks plus the $L\gamma$ subpeaks are listed in Table I. They are related to the three subshell ionization cross sections σ_{L_i} $(i=1,2,3)$ in the following way:

$$\sigma_l = [\sigma_{L_1}(f_{12}f_{23}+f_{13}) + \sigma_{L_2}f_{23} + \sigma_{L_3}]\omega_3 S_{l,3}, \tag{2}$$

$$\sigma_a = [\sigma_{L_1}(f_{12}f_{23}+f_{13}) + \sigma_{L_2}f_{23} + \sigma_{L_3}]\omega_3 S_{a,3}, \tag{3}$$

$$\sigma_\beta = \sigma_{L_1}[\omega_1 S_{\beta,1} + \omega_2 f_{12} S_{\beta,2} + \omega_3(f_{13}+f_{12}f_{23})S_{\beta,3}] + \sigma_{L_2}(\omega_2 S_{\beta,2} + \omega_3 f_{23} S_{\beta,3}) + \sigma_{L_3}\omega_3 S_{\beta,3}, \tag{4}$$

$$\sigma_\gamma = \sigma_{L_1}(\omega_1 S_{\gamma,1} + \omega_2 f_{12} S_{\gamma,2}) + \sigma_{L_2}\omega_2 S_{\gamma,2} \tag{5}$$

$$\sigma_{\gamma_{1+5}} = \sigma_{L_1}\omega_2 f_{12} S_{\gamma_{1+5},2} + \sigma_{L_2}\omega_2 S_{\gamma_{1+5},2} \tag{6}$$

$$\sigma_{\gamma_{2+3}} = \sigma_{L_1}\omega_1 S_{\gamma_{2+3},1} \tag{7}$$

$$\sigma_{\gamma_{4+4'}} = \sigma_{L_1}\omega_1 S_{\gamma_{4+4'},1}, \tag{8}$$

where S_{p_i} is the fraction of the radiative transition to the ith subshell associated with the L_p peak, and f_{ij} are the Coster-Kronig transition probabilities.

From 35 possible combinations of 3 different measured x-ray production cross sections which could be used to extract L_i-subshell ionization cross sections with the above 7 equations, the $\{L\alpha, L\beta, L\gamma\}$, $\{L\alpha, L\gamma_{1+5}, L\gamma_{4+4'}\}$, $\{L\alpha, L\gamma_{1+5}, L\gamma_{2+3}\}$, and $\{L\alpha, L\gamma_{1+5}, L\gamma\}$ are the most com-

TABLE I. Measured L x-ray production cross sections [barn] for in cerium, neodymium, and lutetium by 4- and 6-MeV C^{+2} and 8- and 10-MeV C^{+3} ions.

E_1 (MeV)	Ll	$L\alpha$	$L\beta$	$L\gamma$	$L\gamma_{1+5}$	$L\gamma_{2+3}$	$L\gamma_{4+4'}$
$_{58}$Ce							
4	1.3	26.7	19.1	2.5	1.8	0.7	0.03
6	3.1	71.0	53.3	7.1	4.8	2.3	0.04
8	7.0	163	131	19.7	12.2	7.3	0.13
10	10.3	235	205	32.3	19.6	12.6	0.18
$_{60}$Nd							
4	0.9	19.5	13.1	2.0	1.4	0.56	0.06
6	2.4	66.6	41.1	5.6	4.2	1.2	0.13
8	5.7	143	86.1	11.3	8.5	2.5	0.30
10	10.1	268	156	21.0	15.7	4.9	0.47
$_{71}$Lu						($L\gamma_{2+3+6}$)	
4	0.4	5.0	4.2	0.6	0.49	0.052[a] (0.11)	0.01
6	1.1	20.4	14.4	2.1	1.7	0.18[a] (0.38)	0.04
8	3.1	49.4	32.2	4.5	3.7	0.31[a] (0.75)	0.06
10	6.0	90.3	56.1	7.6	6.3	0.44[a] (1.2)	0.11

[a]For Lu, the $L\gamma_{2+3}$ cross sections—marked in this table with an "a" superscript—were obtained from the $L\gamma_{1+5}$ and $L\gamma_{2+3+6}$ data by the Datz technique [33] that was modified as described in Sec. III A. The $L\gamma_{2+3}$ cross section were derived using the listed $L\gamma_{1+5}$ cross sections instead of $\sigma_{L\gamma_1}=\{0.48,1.64,3.6,6.1\}$ b and the $L\gamma_{2+3}/L\gamma_{4+4'}$ multiplied by $S\gamma_{2+3,1}/S\gamma_{4+4',1}$ corrected for multiple-ionization vacancy; before this correction, with a constant $S\gamma_{2+3,1}/S\gamma_{4+4',1}=7.20$ [37], $\sigma_{L\gamma_{2+3}}=\{0.047,0.16,0.27,0.38\}$ b for single-vacancy ionization of lutetium by $\{4,6,8,10\}$-MeV carbon ions.

mon choices. Detailed descriptions of these 4 methods with their merits and demerits have been made by Jitschin *et al.* [34], Cohen [35], and Singh *et al.* [36]. The first combination often results in negative cross sections. The second combination relies on an accurate knowledge of $L\gamma_{4+4'}$ cross section which even in the best case of Lu is less than 1% of the total L-shell x-ray production cross section (see Table I). Hence we will limit the extraction of L_i-subshell ionization to the $\{L\alpha,L\gamma_{1+5},L\gamma_{2+3}\}$ and $\{L\alpha,L\gamma_{1+5},L\gamma\}$ combinations—i.e., a pair of $L\alpha$ and $L\gamma_{1+5}$ cross sections in conjunction, respectively, with the $L\gamma_{2+3}$ and $L\gamma$ cross sections. Two sets of the L_i-subshell ionization cross sections can be extracted from these two combinations: $\sigma_{L_1'},\sigma_{L_2'},\sigma_{L_3'}\}$ from $\{L\alpha,L\gamma_{1+5},L\gamma_{2+3}\}$ and $\{\sigma_{L_1''},\sigma_{L_2''},\sigma_{L_3''}\}$ from $\{L\alpha,L\gamma_{1+5},L\gamma\}$ cross sections. The weighted average for each L_i subshell,

$$\sigma_{L_i} \equiv w_i\sigma_{L_i'} + (1-w_i)\sigma_{L_i''}, \tag{9}$$

are listed in Tables III–VI as our experimental ionization cross section. The weights $\{w_1,w_2,w_3\}$ with which $\{\sigma_{L_1'},\sigma_{L_2'},\sigma_{L_3'}\}$ enter in this weighted average are defined by the uncertainties $\{\Delta\sigma_{L_1'},\Delta\sigma_{L_2'},\Delta\sigma_{L_3'}\}$ and $\{\Delta\sigma_{L_1''},\Delta\sigma_{L_2''},\Delta\sigma_{L_3''}\}$ with which the L_i-subshell ionization cross sections are derived from $\{L\alpha,L\gamma_{1+5},L\gamma_{2+3}\}$ and $\{L\alpha,L\gamma_{1+5},L\gamma\}$ combinations: $w_i \equiv (\Delta\sigma_{L_i''})^2/[(\Delta\sigma_{L_i''})^2 + (\Delta\sigma_{L_i''})^2]$. The values of w_i are displayed in Tables III–VI. The $\Delta\sigma_{L_1'}$ error in the $\sigma_{L_1'}$ determination is significantly smaller than in the $\sigma_{L_1''}$ because by Eq. (7) $\sigma_{L_1'}$ depends solely on the $L\gamma_{2+3}$. The large $\Delta\sigma_{L_1''}$ error in $\sigma_{L_1''}$ derived from Eq. (5) reflects the uncertainties in the extracted σ_{L_2} as well as σ_{L_1}. Hence with w_1 values in the 0.87–0.99 range the weighted average for σ_{L_1} is equal, within a couple of percents, to $\sigma_{L_1'}$ extracted from the $\{L\alpha,L\gamma_{1+5},L\gamma_{2+3}\}$ combination. On the other hand, with comparable errors for the extraction of L_2 and L_3 cross sections from both combinations, w_2 and w_3 are about 0.6 and 0.5. These values of w_2 and w_3 are essentially equal to the arithmetic average of 0.5 for these two combinations. Indeed, the L_2 and L_3 cross sections obtained from either combination are the same to within a few percent. Therefore, in effect, the L_i-subshell ionization cross sections could have been extracted *only* from the $\{L\alpha,L\gamma_{1+5},L\gamma_{2+3}\}$ combination as reliably as the weighted average of these cross sections is obtained by the $\{L\alpha,L\gamma_{1+5},L\gamma_{2+3}\}$ and $\{L\alpha,L\gamma_{1+5},L\gamma\}$ methods.

A. Determination of $L\gamma_{2+3}$ for Lu using a revised Datz technique

Ce and Nd have no electron in the O_{IV} orbital and thus their spectra have no contribution from the $L\gamma_6$ line. For Lu, with our Si(Li) detector, $L\gamma_{2+3+6}$ is observed as a single peak and so the contribution of the $L\gamma_6$ line should be properly subtracted from the composite $L\gamma_{2+3+6}$ line to get the x-ray production peak of $L\gamma_{2+3}$. According to the technique of Datz *et al.* [33], a straight-line fit to the intensity ratio $y \equiv L\gamma_{2+3+6}/L\gamma_1$ plotted against the $x \equiv L\gamma_{4+4'}/L\gamma_1$ yields the ratio of the $L\gamma_6$ intensity relative to the $L\gamma_1$ intensity as an

intercept of that line with the y axis. We apply this technique with the following revisions.

(1) Instead of $L\gamma_1$ that was originally proposed [33], the unresolved sum $L\gamma_{1+5}$ of $L\gamma_1$ and $L\gamma_5$ is used because $L\gamma_1$ would require an error-propagating subtraction of $L\gamma_5$ from $L\gamma_{1+5}$. This revision reduces the statistical error in using the technique of Datz *et al.* [33].

(2) Based on the unnumbered straight-line equation on p. 193 of Ref. [33], the Datz plot should in principle be made against $x \equiv (S\gamma_{2+3,1}/S\gamma_{4+4'})(L\gamma_{4+4'}/L\gamma_{1+5})$. When multiple ionization is minimal, as it was in ionization of gold by protons [33], $S\gamma_{2+3,1}/S\gamma_{4+4'}$ remains essentially the same for all measurements on a singly-ionized target atom. A *constant* value of $S\gamma_{2+3,1}/S\gamma_{4+4'}$ affects the slope of a fitted straight line in a plot of $y \equiv L\gamma_{2+3+6}/L\gamma_{1+5}$ vs the revised and proper definition of x, but has no bearing on the value of the extracted intercept of y at $x=0$. Thus, $S\gamma_{2+3,1}/S\gamma_{4+4'}$ could have been 5.62—as calculated per Ref. [37] for singly ionized Au of the experiment of Datz *et al.*—or simply set to be 1 as routinely has been done whenever the Datz plot was shown in the literature.

However, while $S\gamma_{2+3,1}/S\gamma_{4+4',1}$ is a constant known from the adopted single-hole values—which in our case equals 7.20 based on $S\gamma_{2+3,1}$ and $S\gamma_{4+4',1}$ for Lu listed in Table II per Ref. [37]—this may not be the case when multiple ionization by heavy ions affects these rates to a different degree at different ion energies. Indeed, due to multiple ionization, $S\gamma_{2+3,1}/S\gamma_{4+4',1}$ varies with the carbon ion energy as will be calculated in Sec. III C 1.

(3) The plotted points have more uncertainty in the x coordinates (due to the weakest line of $L\gamma_{4+4'}$) than along the y coordinate; hence straight-line fits shown in Fig. 3 were performed with the program GENLS [38], which accounts for both x and y errors.

In Fig. 3, the measured values of $L\gamma_{2+3+6}/L\gamma_{1+5}$ are drawn at x defined with both single- and multiple-hole values for $S\gamma_{2+3,1}/S\gamma_{4+4',1}$ as listed in Table II. Such data shall, as required by the correct application of the Datz technique, be fitted with a straight line. In practice, the straight-line fit gave us a smaller sum of the squared deviations than fits with a parabola. Although intercepts of the fitted straight lines for single (0.13 ± 0.03) and multiple (0.12 ± 0.04) vacancy cases are close, we propose that the Datz plot ought to be made against $x=(S\gamma_{2+3,1}/S\gamma_{4+4',1})(L\gamma_{4+4'}/L\gamma_{1+5})$ whenever corrections for multiple ionization are made to the values of $S\gamma_{2+3,1}$ and $S\gamma_{4+4',1}$. For our collision system, as shown in the next section, the probability of outer-shell ionization is relatively small (0.15 on the average and not exceeding 0.30) and weakly dependent on the projectile energy. Hence L_1-subshell ionization cross sections extracted with the revised Datz technique are merely 10% greater than if obtained with the standard Datz technique of Ref. [33]. For L_2 and L_3 subshells, the revised and standard calculations are essentially the same. However, this may not be the case for collision systems in which multiple ionization is larger and more strongly varied with the projectile energy.

B. Effect of a different choice for single-hole atomic parameters on the extracted ionization cross sections

It was noted by Cohen [35] that the disagreement of the ionization data with the predictions of different theoretical

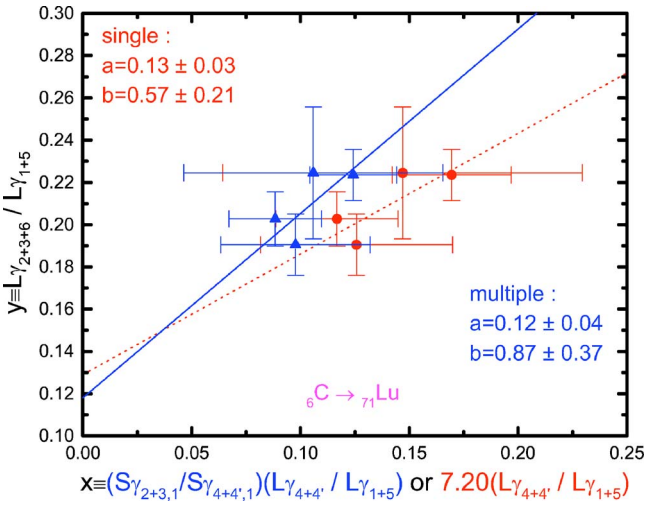

FIG. 3. (Color online) The Datz plot [33] revised as described in the Sec. III A. The intercepts of 0.13 (single vacancy) and 0.12 (multiple vacancies) from the $y=a+b\cdot x$ fits [38] are used to untangle the cross section for $L\gamma_{2+3}$ x-ray production from the $L\gamma_{2+3+6}$ measurement.

models might depend to some extent on the use of different atomic parameters. To assess this variation, the L_i-subshell ionization cross sections have been calculated using different sets of the atomic parameters. For the fluorescence yields and Coster-Kronig (CK) transition rates we have tried values recommended by Krause [39], Puri *et al.* [40], and Campbell [41]; for the branching ratios we have used the tables of Scofield [42] as well as the tables of Campbell and Wang [37]. The cross section values obtained using all permutations of different sets of atomic parameters from these references agree with each other to within 10%. We settled on Refs. [37] and [41] as the most reliable combination of single-hole atomic parameters. They are listed in the second column of Table II. L_i-subshell ionization cross sections extracted with these single-vacancy atomic parameters are displayed in Table III.

C. Multiple-ionization effects

Multiple-ionization can substantially change the values of fluorescence yields as well as Coster-Kronig and Auger transition rates. Due to the loss of electrons from the outer shells, the Coster-Kronig–Auger rates, which involve two electrons, will be more affected than the radiative rate which is a single-electron process. Another consequence of the loss of electrons from the outer shells is the reduction of screening of the nucleus which in turn increases the binding energy of the electrons. This slight increase in binding energy could sometimes block the possible CK transitions altogether. In the following subsection, the change of radiative and nonradiative widths due to these two effects will be discussed in details. At the conclusion of this section we will compare the ionization cross sections extracted by these procedures.

1. Change of parameters according to statistical scaling of Larkins with calculated probabilities for outer-shell ionization according to Ref. [44]

The decrease of the widths for both radiative as well as nonradiative transitions due to the reduction of the number of

TABLE II. Single-hole atomic parameters for the fluorescence and CK yields from Campbell [41] and for the radiative widths from Campbell and Wang [37]. Where the recommended values were not available in [41], the DHS values were taken from that reference. Multiple-hole atomic parameters based on the statistical scaling of Larkins [43] evaluated with the ionization probabilities of Sulik *et al.* [44], and further corrected for closure of CK transitions [61].

		Statistical scaling [43]				Closed CK [61]
$_{58}$Ce	Single-hole [37,41]	4 MeV	6 MeV	8 MeV	10 MeV	10 MeV
ω_1	0.061	0.082	0.081	0.080	0.079	0.084
ω_2	0.119	0.144	0.145	0.146	0.146	0.146
ω_3	0.119	0.136	0.137	0.140	0.141	0.141
f_{12}	0.190	0.182	0.187	0.194	0.199	0.147
f_{13}	0.250	0.304	0.313	0.324	0.333	0.355
f_{23}	0.158	0.144	0.151	0.160	0.167	0.167
Γ_1	0.2402	0.2192	0.2176	0.2146	0.2129	0.2129
Γ_2	0.4134	0.3843	0.3807	0.3746	0.3707	0.3707
Γ_3	0.3850	0.3580	0.3546	0.3489	0.3452	0.3452
$\Gamma_{\alpha,3}$	0.3145	0.3058	0.3013	0.2944	0.2895	0.2895
$\Gamma_{\gamma 1+5,2}$	0.0628	0.0438	0.0452	0.0468	0.0484	0.0484
$\Gamma_{\gamma,1}$	0.0519	0.0384	0.0394	0.0405	0.0416	0.0416
$\Gamma_{\gamma,2}$	0.0632	0.0438	0.0452	0.0468	0.0484	0.0484
$\Gamma\gamma_{2+3,1}$	0.0447	0.0312	0.0322	0.0334	0.0344	0.0344
$S_{\alpha,3}$	0.8169	0.8543	0.8498	0.8437	0.8386	0.8386
$S_{\beta,1}$	0.7744	0.8250	0.8191	0.8111	0.8045	0.8045
$S_{\beta,2}$	0.8241	0.8621	0.8575	0.8513	0.8460	0.8460
$S_{\beta,3}$	0.1509	0.1121	0.1169	0.1231	0.1285	0.1285
$S_{\gamma,1}$	0.2161	0.1750	0.1809	0.1889	0.1955	0.1955
$S_{\gamma,2}$	0.1529	0.1139	0.1187	0.1250	0.1304	0.1304
$S_{\gamma 1+5,2}$	0.1519	0.1139	0.1187	0.1250	0.1304	0.1304
$S_{\gamma 2+3,1}$	0.1861	0.1422	0.1479	0.1554	0.1618	0.1618
$S_{\gamma 4+4',1}$	0.0300	0.0327	0.0330	0.0335	0.0337	0.0337

		Statistical scaling [43]				Closed CK [61]	
$_{60}$Ne	Single-hole [37,41]	4 MeV	6 MeV	8 MeV	10 MeV	8 MeV	10 MeV
ω_1	0.067	0.088	0.087	0.086	0.085	0.091	0.090
ω_2	0.136	0.163	0.164	0.165	0.164	0.164	0.165
ω_3	0.134	0.151	0.153	0.155	0.157	0.155	0.157
f_{12}	0.190	0.189	0.195	0.201	0.206	0.154	0.158
f_{13}	0.250	0.309	0.319	0.329	0.337	0.348	0.358
f_{23}	0.158	0.139	0.146	0.154	0.160	0.154	0.160
Γ_1	0.2844	0.2616	0.2588	0.2564	0.2545	0.2564	0.2545
Γ_2	0.4913	0.4609	0.4551	0.4499	0.4457	0.4499	0.4457
Γ_3	0.4561	0.4280	0.4225	0.4176	0.4137	0.4176	0.4137
$\Gamma_{\alpha,3}$	0.3721	0.3659	0.3591	0.3526	0.3473	0.3526	0.3473
$\Gamma_{\gamma 1+5,2}$	0.0756	0.0527	0.0544	0.0564	0.0583	0.0564	0.0583
$\Gamma_{\gamma,1}$	0.0618	0.0456	0.0468	0.0482	0.0495	0.0482	0.0495
$\Gamma_{\gamma,2}$	0.0761	0.0527	0.0544	0.0564	0.0583	0.0564	0.0583
$\Gamma\gamma_{2+3,1}$	0.0535	0.0373	0.0385	0.0399	0.0412	0.0399	0.0412
$S_{\alpha,3}$	0.8159	0.8548	0.8499	0.8444	0.8394	0.8444	0.8394
$S_{\beta,1}$	0.7725	0.8257	0.8191	0.8119	0.8054	0.8119	0.8054
$S_{\beta,2}$	0.8223	0.8618	0.8567	0.8510	0.8459	0.8510	0.8459

TABLE II. (*Continued.*)

		Statistical scaling [43]				Closed CK [61]	
$_{60}$Ne	Single-hole [37,41]	4 MeV	6 MeV	8 MeV	10 MeV	8 MeV	10 MeV
$S_{\beta,3}$	0.1524	0.1123	0.1174	0.1232	0.1283	0.1232	0.1283
$S_{\gamma,1}$	0.2173	0.1743	0.1809	0.1881	0.1946	0.1881	0.1946
$S_{\gamma,2}$	0.1549	0.1144	0.1196	0.1254	0.1307	0.1254	0.1307
$S_{\gamma 1+5,2}$	0.1540	0.1144	0.1196	0.1254	0.1307	0.1254	0.1307
$S_{\gamma 2+3,1}$	0.1882	0.1426	0.1488	0.1557	0.1619	0.1557	0.1619
$S_{\gamma 4+4',1}$	0.0292	0.0317	0.0321	0.0324	0.0326	0.0324	0.0326

		Statiscal scaling [43]				Closed CK [61]			
$_{71}$Lu	Single-hole [37,41]	4 MeV	6 MeV	8 MeV	10 MeV	4 MeV	6 MeV	8 MeV	10 MeV
ω_1	0.140	0.149	0.148	0.146	0.145	0.161	0.160	0.159	0.157
ω_2	0.256	0.296	0.296	0.296	0.296	0.296	0.296	0.296	0.296
ω_3	0.231	0.259	0.260	0.261	0.262	0.259	0.260	0.261	0.262
f_{12}	0.125	0.160	0.162	0.165	0.168	0.093	0.094	0.096	0.098
f_{13}	0.320	0.323	0.328	0.334	0.339	0.349	0.354	0.361	0.368
f_{23}	0.138	0.112	0.114	0.118	0.121	0.112	0.114	0.118	0.121
Γ_1	0.6480	0.5995	0.5985	0.5978	0.5969	0.5995	0.5985	0.5978	0.5969
Γ_2	1.1495	1.093	1.090	1.087	1.084	1.093	1.090	1.087	1.084
Γ_3	1.0327	0.9826	0.9800	0.9775	0.9745	0.9826	0.9800	0.9775	0.9745
$\Gamma_{\alpha,3}$	0.8326	0.8295	0.8249	0.8190	0.8129	0.8295	0.8249	0.8190	0.8129
$\Gamma_{\gamma 1+5,2}$	0.1854	0.1332	0.1359	0.1400	0.1440	0.1332	0.1359	0.1400	0.1440
$\Gamma_{\gamma,1}$	0.1434	0.1080	0.1098	0.1126	0.1153	0.1080	0.1098	0.1126	0.1153
$\Gamma_{\gamma,2}$	0.1864	0.1332	0.1359	0.1400	0.1440	0.1332	0.1359	0.1400	0.1440
$\Gamma\gamma_{2+3,1}$	0.1260	0.0905	0.0923	0.0951	0.0978	0.0905	0.0923	0.0951	0.0978
$S_{\alpha,3}$	0.8062	0.8443	0.8417	0.8379	0.8342	0.8443	0.8417	0.8379	0.8342
$S_{\beta,1}$	0.7613	0.8199	0.8166	0.8117	0.8069	0.8199	0.8166	0.8117	0.8069
$S_{\beta,2}$	0.8155	0.8548	0.8521	0.8481	0.8442	0.8548	0.8521	0.8481	0.8442
$S_{\beta,3}$	0.1574	0.1178	0.1204	0.1244	0.1283	0.1178	0.1204	0.1244	0.1283
$S_{\gamma,1}$	0.2213	0.1801	0.1834	0.1883	0.1931	0.1801	0.1834	0.1883	0.1931
$S_{\gamma,2}$	0.1622	0.1219	0.1247	0.1288	0.1328	0.1219	0.1247	0.1288	0.1328
$S_{\gamma 1+5,2}$	0.1613	0.1219	0.1247	0.1288	0.1328	0.1219	0.1247	0.1288	0.1328
$S_{\gamma 2+3,1}$	0.1943	0.1510	0.1542	0.1591	0.1639	0.1510	0.1542	0.1591	0.1639
$S_{\gamma 4+4',1}$	0.0270	0.0291	0.0292	0.0291	0.0293	0.0292	0.0292	0.0292	0.0293

electrons available for a given transition can be calculated using the statistical scaling of Larkins [43]. The fraction of available electrons in a particular shell is directly related to the ionization probability of that shell which may either be measured experimentally or calculated theoretically as per the condition of the experiment. It is assumed that, for a given projectile energy, each electron in a particular shell is ionized with the same probability P evaluated according to the geometrical model of Sulik *et al.* [44]. This model, based on the binary encounter approximation, has been adopted or tested in many works [13,45–61]. Its P values are—as for any scheme based on a first-order perturbation theory and despite a misleading claim [13,55–58] that the model derives from a nonperturbative approach which the BEA is not—in doubt when collisions are not sufficiently fast for Z_1/v_1 to fall below 1, where Z_1 and $v_1=6.351$ $[E_1\ (\mathrm{MeV})/A_1\ (\mathrm{amu})]^{1/2}$ are the projectile's atomic number and velocity. Furthermore, the BEA is generally successful in the limited range of the projectile velocity v_1 where v_1 is comparable with the orbital velocity v_{2S} of the electron in the ionized shell. In fact, although better than the standard BEA [62] as gauged [45] against the coupled-state calculations [63], the P of Ref. [44] falls below and above the CUSCAR predictions when, respectively, $v_1<v_{2S}$ and $v_1>v_{2S}$ [13,51,54,56,58–60]. Although definitely better than the results of the classical Monte Carlo calculations [52,54,60], P of Ref. [44] progressively exceeds the data when its value increases above 0.4 [44,46]. It has been suggested that this gap between the measurements and results of Ref. [44] could be explained by fast refilling of outer-shell vacancies by the

valence-band electrons in solid targets [57]. For our data, the predictions of the geometrical model of Sulik *et al.* [44] deem to be applicable because Z_1/v_1 hovers around 1 and satisfactory since—according to this model—the probabilities for the removal of an electron from the M or N shells are less than 0.3—i.e., in the range where agreement with experiment is generally good [44–60].

The L-shell decay widths are mainly modified by the multiple ionization in the M and N shells. The influence of the multiple ionization in the O shell is small ($\leqslant 3\,\%$) [59] due to the small contribution of the transition involving O-shell electrons to the L-shell decay widths and so its contribution has been neglected. Figure 4 displays ionization probabilities for M and N shells of Ce, Nd, and Lu targets bombarded by carbon ions calculated according to the formula of Sulik *et al.* [44]. Using the theoretical values of radiative rates from Campbell and Wang [37], Coster-Kronig and Auger rates from Chen *et al.* [64] and calculated ionization probabilities for the M and N shells shown in Fig. 4, the modified L-subshell decay widths of all the possible channels for the individual radiative $\Gamma^R(L_iX)$, Coster-Kronig $\Gamma^{CK}(L_iL_jX)$ and Auger $\Gamma^A(L_iM_iX)$ processes were modified according to Banaś *et al.* [61] where $X=M$, N and $j>i$. Finally, the fluorescence yields and the Coster-Kronig transition rates due to multiple ionization were calculated. The modified L-shell atomic parameters of Ce, Nd, and Lu are listed in Table II under the heading "statistical scaling" [43,44], and the L_i-subshell ionization cross sections extracted with these parameters are listed in Table IV.

2. *Further change of atomic parameters due to closing of CK transitions according to Ref. [61]*

Multiple ionization increases the binding energy of the inner-shell electrons due to the reduction in screening. Low-energy CK transitions are particularly affected by such increase of binding, and sometimes such transitions are totally closed. Such closure of the CK transitions changes the decay widths and thus modifies the fluorescence and Coster-Kronig yields. The change in binding energy of the electrons due to the vacancy formation was calculated following the prescription of Banaś *et al.* [61]. The CK transition is identified as

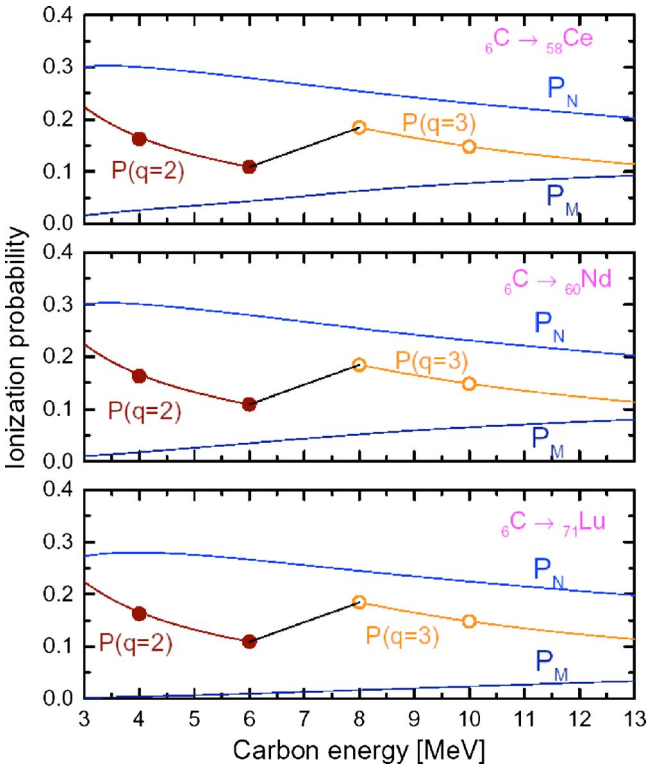

FIG. 4. (Color online) Probabilities for the outer shells ionization: P_M and P_N according to the BEA geometrical model of Sulik *et al.* [44] plus $P(q=2)$ and $P(q=3)$ of Eq. (11) for ionization of every electron from a manifold of outer shells according to Lapicki *et al.* [66,69]. These probabilities are used for the multiple-ionization correction of the single-hole atomic parameters as described in the Secs. III C 1 and III C 3. For the collision system of our experiment—with $Z_2=58-71$ elements bombarded by the carbon ions of $4<v_1<6$ velocities—$v_1<v_{2M}$ and $v_1>v_{2N}$. Based on Refs. [13,51,54,56,58–60], P_M and P_N of Sulik *et al.* [44] are, respectively, smaller and greater than what would have been calculated in Trautmann's CUSCAR theory [11,13]. The probability for ionization of an outer-shell electron [66,69] is then closely bracketed by P_M and P_N predicted by the CUSCAR theory.

TABLE III. L_i-subshell ionization cross sections [barn] for 4 and 6 MeV C^{+2} and 8 and 10 MeV C^{+3} on Ce, Nd, and Lu extracted from the measured x-ray production cross sections using fluorescence and CK yields of Campbell [41] and radiative rates of Campbell and Wang [37]. The cross sections listed in bold print are the weighted average of ionization cross sections, extracted from two combinations of $L\gamma_{2+3}$ and $L\gamma$ with the same $\{L\alpha, L\gamma_{1+5}\}$ pair of peak cross sections. They are followed by the weight w_i with which the L_i extracted from $\{L\alpha, L\gamma_{1+5}, L\gamma_{2+3}\}$ contributed to this weighted average.

	4			6			8			10		
	L_1	L_2	L_3	L_1	L_2	L_3	L_1	L_2	L_3	L_1	L_2	L_3
$_{58}$**Ce**	**61.0**	**88.5**	**245**	**200**	**229**	**642**	**633**	**558**	**1419**	**1090**	**884**	**1989**
w_i	0.94	0.63	0.51	0.91	0.63	0.51	0.88	0.63	0.51	0.87	0.63	0.51
$_{60}$**Nd**	**44.1**	**58.7**	**157**	**95.1**	**183**	**554**	**198**	**369**	**1195**	**386**	**678**	**2240**
w_i	0.91	0.63	0.51	0.95	0.63	0.51	0.94	0.63	0.51	0.94	0.63	0.51
$_{71}$**Lu**	**1.78**	**11.6**	**24.4**	**6.08**	**40.1**	**101**	**10.2**	**87.6**	**247**	**14.3**	**149**	**455**
w_i	0.97	0.58	0.52	0.97	0.58	0.51	0.98	0.58	0.51	0.99	0.58	0.51

TABLE IV. *L*-subshell ionization cross sections [barn] for 4 and 6 MeV C^{+2} and 8 and 10 MeV C^{+3} on Ce, Nd, and Lu extracted from the measured x-ray production cross sections using fluorescence and CK yields of Campbell [41] and radiative rates of Campbell and Wang [37], corrected for the multiple ionization using the statistical scaling of Larkins [43] ionization probabilities of Sulik *et al.* [44] with none of the CK transitions closed. The cross sections listed in bold print are the weighted average of ionization cross sections, extracted from two combinations of $L\gamma_{2+3}$ and $L\gamma$ with the same $\{L\alpha, L\gamma_{1+5}\}$ pair of peak cross sections. They are followed by the weight w_i with which the L_i extracted from $\{L\alpha, L\gamma_{1+5}, L\gamma_{2+3}\}$ contributed to this weighted average. Also shown are the multiple-ionization (MI) factors calculated as the ratios of ionization cross sections extracted with-to-without correction of the atomic parameters for MI effect.

	4			6			8			10		
	L_1	L_2	L_3	L_1	L_2	L_3	L_1	L_2	L_3	L_1	L_2	L_3
$_{58}$Ce	**59.2**	**99.6**	**197**	**189**	**246**	**513**	**576**	**561**	**1097**	**963**	**846**	**1513**
w_i	0.93	0.60	0.51	0.90	0.61	0.51	0.87	0.62	0.52	0.86	0.62	0.52
MI	0.97	1.12	0.80	0.95	1.07	0.80	0.91	1.01	0.77	0.88	0.96	0.76
$_{60}$Nd	**44.1**	**67.0**	**128**	**92.5**	**196**	**452**	**186**	**377**	**970**	**354**	**657**	**1803**
w_i	0.90	0.61	0.52	0.94	0.62	0.51	0.94	0.63	0.51	0.93	0.63	0.51
MI	1.00	1.14	0.82	0.97	1.07	0.82	0.94	1.02	0.81	0.92	0.97	0.80
$_{71}$Lu	**2.40**	**13.6**	**20.4**	**8.23**	**46.1**	**84.5**	**13.8**	**97.6**	**208**	**19.2**	**161**	**384**
w_i	0.93	0.60	0.53	0.93	0.61	0.52	0.95	0.61	0.52	0.97	0.61	0.52
MI	1.35	1.17	0.84	1.35	1.16	0.84	1.35	1.11	0.84	1.34	1.08	0.84

closed if the calculated electron kinetic energy is found to be negative. The diagram energies for the CK electrons were taken from Chen *et al.* [65]. Using the calculated ionization probabilities for the *M* and *N* shells of Ce, Nd, and Lu targets bombarded by carbon ion (as shown in Fig. 4 according to Ref. [44]), we found that only the L_1-L_2N_1 CK transition is closed for Ce at 10 MeV and for Nd target at 8 and 10 MeV. In Lu, the L_1-$L_2N_{2,3}$ CK transitions are closed at all energies. Hence the major effect of multiple ionization on the fluorescence and Coster-Kronig yields was found only for the L_1 subshell. The modified *L*-shell atomic parameters due to closing of CK transitions for all three elements are listed in Tables III under the heading "closed CK" [61], and the L_i-subshell ionization cross sections extracted with these parameters are listed in Table V.

3. Alternative method of accounting for multiple ionization according to Refs. [66] and [69]

In parallel with the development of the BEA geometrical model of Sulik *et al.* [44] for calculation of the probability of ionization from outer subshells, Lapicki *et al.* [66] proposed to correct single-hole fluorescence yields ω_i^0 using a simplified assumption that each electron in a manifold of outer subshells is ionized with an identical probability *P* so that the fluorescence yields ω_i corrected for multiple ionization becomes

$$\omega_i = \omega_i^0/[1 - P(1 - \omega_i^0)]. \tag{10}$$

According to Eq. (A3) in [66] derived from the classical cross section of Thomson [67] and after the replacement of Z_1 with the projectile charge state *q* [68],

$$P = q^2(1 - 0.225/v_1^2)/1.8v_1^2. \tag{11}$$

This probability is shown in Fig. 4 for comparison with the probabilities obtained in the model of Sulik *et al.* [44]. As further stated by Lapicki *et al.* [69], with all nonradiative transitions involving two electrons narrowed by the same factor $(1-P)^2$, the single-hole CK transitions f_{ij}^0 are reduced to

$$f_{ij} = f_{ij}^0(1 - P)^2, \tag{12}$$

while the fractional rates S_{ij} remain unchanged because both partial and total nonradiative widths Γ are narrowed by identical factors.

The L_i-subshell ionization cross sections extracted with the fluorescence and CK yields modified for multiple ionization in this manner are listed in Table VI. Tables IV–VI display the multiple-ionization (MI) factor defined as the ratio of the ionization cross section extracted with the atomic parameters corrected—as described above, respectively, in Secs. III C 1, III C 2, and III C 3—for multiple-ionization to ionization cross sections shown in Table III as derived with single-hole atomic parameters listed in the second column of Table II. It is evident that although multiple ionizations can significantly affect the atomic parameters, the MI factors reflect a competition between the reduction of one-electron radiative rates and the greater reduction of nonradiative rates which manifests itself in the struggle of the enhancement of the fluorescence yields versus the reduction of the nonradiative yields in Eqs. (2)–(8). The net balance between these large but opposite changes is that the ionization cross sections extracted with the atomic parameters corrected substantially for multiple ionization are typically merely within a few to 35% of the cross sections derived with the single-hole atomic parameters.

Assessing the approach in which the effect of multiple ionizations was calculated with the model of Sulik *et al.* [44] and an equation of Banaś *et al.* [61] to identify closed CK transitions (see Table V) versus the alternative treatment of Lapicki *et al.* [66,69] (see Table VI), we find that L_1 ionization cross sections extracted with multiple-hole ionization

TABLE V. *L*-subshell ionization cross sections [barn] for 4 and 6 MeV C^{+2} and 8 and 10 MeV C^{+3} on Ce, Nd, and Lu extracted from the measured x-ray production cross sections using fluorescence and CK yields of Campbell [41] and radiative rates of Campbell and Wang [37], corrected for the multiple ionization using the statistical scaling of Larkins [43] ionization probabilities of Sulik *et al.* [44] with some (see the numbers in *italic*) of the CK transitions closed [61]. The cross sections listed in bold print are the weighted average of ionization cross sections, extracted from two combinations of $L\gamma_{2+3}$ and $L\gamma$ with the same $\{L\alpha, L\gamma_{1+5}\}$ pair of peak cross sections. They are followed by the weight w_i with which the L_i extracted from $\{L\alpha, L\gamma_{1+5}, L\gamma_{2+3}\}$ contributed to this weighted average. Also shown are the multiple-ionization (MI) factors calculated as the ratios of ionization cross sections extracted with-to-without correction of the atomic parameters for MI effect.

	4			6			8			10		
	L_1	L_2	L_3	L_1	L_2	L_3	L_1	L_2	L_3	L_1	L_2	L_3
$_{58}$Ce	**59.2**	**99.6**	**197**	**189**	**246**	**513**	**576**	**561**	**1097**	***906***	***903***	***1512***
w_i	0.93	0.60	0.51	0.90	0.61	0.51	0.87	0.62	0.52	*0.86*	*0.59*	*0.52*
MI	0.97	1.12	0.80	0.95	1.07	0.80	0.91	1.01	0.77	*0.83*	*1.02*	*0.76*
$_{60}$Nd	**44.1**	**67.0**	**128**	**92.5**	**196**	**452**	***176***	***387***	***970***	***334***	***677***	***1803***
w_i	0.90	0.61	0.52	0.94	0.62	0.51	*0.94*	*0.59*	*0.51*	*0.93*	*0.60*	*0.51*
MI	1.00	1.14	0.82	0.97	1.07	0.82	*0.89*	*1.05*	*0.81*	*0.87*	*1.00*	*0.80*
$_{71}$Lu	***2.22***	***13.8***	***20.4***	***7.61***	***46.8***	***84.5***	***12.7***	***99.9***	***208***	***17.7***	***163***	***383***
w_i	*0.93*	*0.56*	*0.53*	*0.93*	*0.56*	*0.52*	*0.95*	*0.56*	*0.52*	*0.97*	*0.56*	*0.52*
MI	*1.25*	*1.19*	*0.84*	*1.25*	*1.17*	*0.84*	*1.25*	*1.14*	*0.84*	*1.24*	*1.09*	*0.84*

according to [44,61] fluctuate 25% below and above single-hole results while the treatment of Lapicki *et al.* [66,69] yields 10%–15% lower cross sections. For L_2, Refs. [44,61] give cross sections that are 1%–19% above while per [62,65] extracted ionization cross sections are 7%–13% below the single-hole results. For L_3, both approaches lower ionization cross sections—by 16%–24% per [44,61] and uniformly by about 10% according to [66,69]. With these trends plus the L_2 and even more so the L_3 subshells dominating the total *L*-shell ionization, both approaches lead to virtually identical *L*-shell ionization cross sections; both accounts for multiple ionizations lower cross sections obtained with single-hole parameters by no more than 10%.

Neither of these two methods is further modified for vacancy rearrangements occurring after the time of production of a multihole atom and prior to the time of x-ray emission. Quantitative studies by Horvat *et al.* [53] of the effect of such rearrangements on $K\alpha$ and $K\beta$ spectra in fast (10 MeV/u) and quite symmetric ($Z_1/Z_2 \geqslant 1/3$) collisions require information about thousands of possible decay branches for an original state of a multiply ionized atom and are necessary for a better reproduction of these spectra. To explain *L* x-ray satellites and hypersatellites produced in more symmetric ($Z_1/Z_2 \geqslant 0.4$) collisions, multiconfiguration Dirac-Fock calculations for over 3000 x-ray transitions are required for just two original vacancy arrangements [70].

TABLE VI. *L*-subshell ionization cross sections [barn] for 4 and 6 MeV C^{+2} and 8 and 10 MeV C^{+3} on Ce, Nd, and Lu extracted from the measured x-ray production cross sections using fluorescence and CK yields of Campbell [41] and radiative rates of Campbell and Wang [37], corrected for the multiple ionization according to Lapicki *et al.* [66,69] [see Eqs. (10)–(13)]. The cross sections listed in bold print are the weighted average of ionization cross sections, extracted from two combinations of $L\gamma_{2+3}$ and $L\gamma$ with the same $\{L\alpha, L\gamma_{1+5}\}$ pair of peak cross sections. They are followed by the weight w_i with which the L_i extracted from $\{L\alpha, L\gamma_{1+5}, L\gamma_{2+3}\}$ contributed to this weighted average. Also shown are the multiple-ionization (MI) factors calculated as the ratios of ionization cross sections extracted with-to-without correction of the atomic parameters for MI effect.

	4			6			8			10		
	L_1	L_2	L_3	L_1	L_2	L_3	L_1	L_2	L_3	L_1	L_2	L_3
$_{58}$Ce	**51.7**	**78.8**	**217**	**179**	**214**	**597**	**524**	**502**	**1261**	**938**	**819**	**1832**
w_i	0.94	0.59	0.50	0.91	0.60	0.50	0.88	0.59	0.50	0.87	0.60	0.51
MI	0.85	0.89	0.89	0.90	0.93	0.93	0.83	0.90	0.89	0.86	0.93	0.92
$_{60}$Nd	**37.4**	**52.6**	**141**	**85.5**	**169**	**512**	**164**	**321**	**1037**	**333**	**609**	**2004**
w_i	0.91	0.60	0.50	0.95	0.61	0.50	0.94	0.59	0.50	0.94	0.60	0.50
MI	0.85	0.90	0.90	0.90	0.92	0.92	0.83	0.87	0.87	0.86	0.90	0.89
$_{71}$Lu	**1.53**	**10.2**	**22.0**	**5.51**	**37.0**	**94.0**	**8.59**	**76.1**	**217**	**12.5**	**134**	**411**
w_i	0.97	0.56	0.51	0.97	0.57	0.51	0.98	0.55	0.50	0.99	0.56	0.50
MI	0.86	0.88	0.90	0.91	0.92	0.93	0.84	0.87	0.88	0.87	0.90	0.90

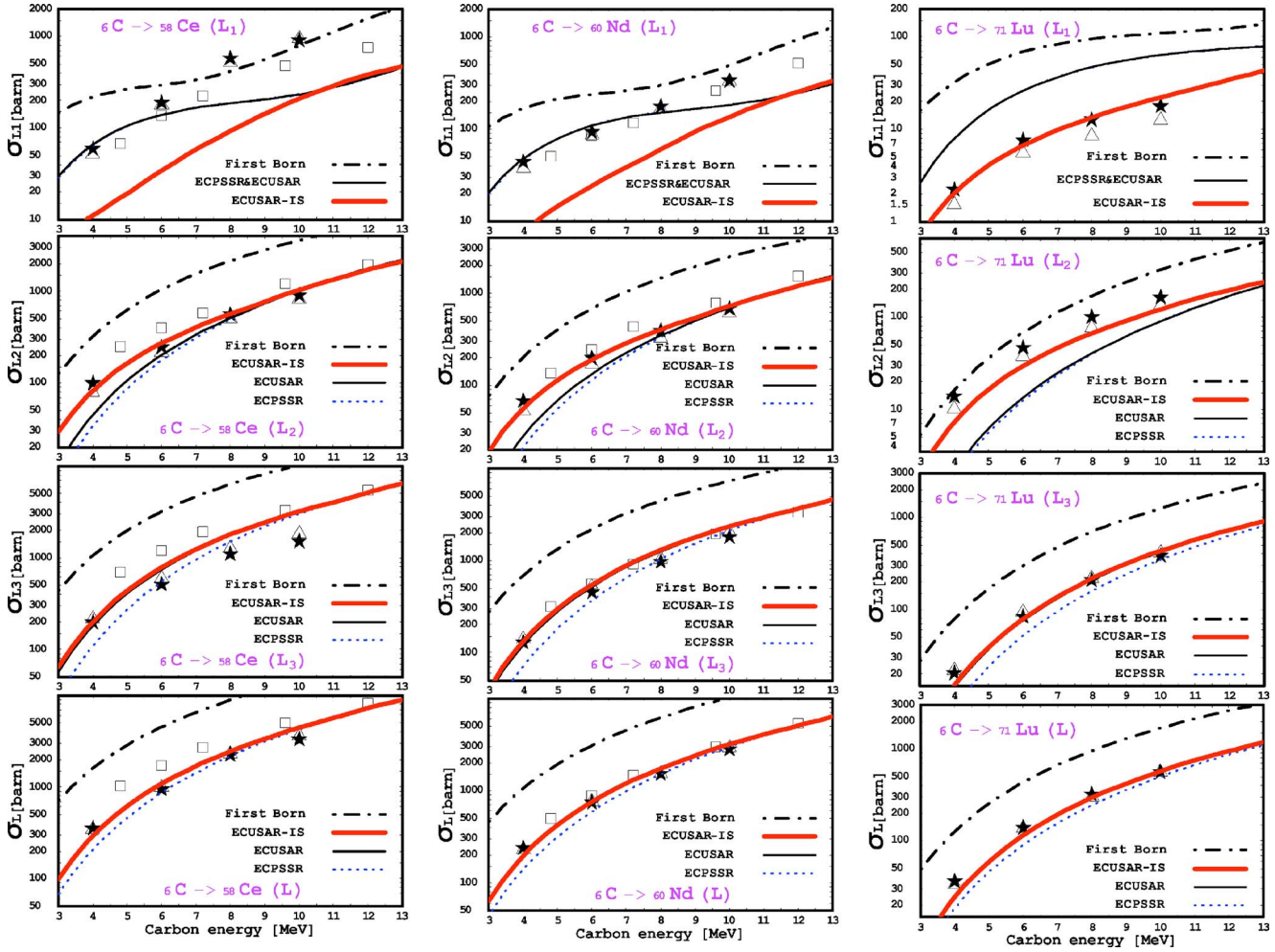

FIG. 5. (Color online) Comparison of the L_1, L_2, L_3, L-shell ionization cross sections for Ce and Nd from Ref. [78] (squares) and of the data extracted for our x-ray production measurements for Ce, Nd, and Lu according to Refs. [44,61] (stars) and Refs. [64,69] (triangles) with the first Born [5,8], ECPSSR [9,10], ECUSAR [12], and ECUSAR-IS [see Eq. (13)] theories.

Continuing such studies on $K\alpha$ spectra for more nearly symmetric ($Z_1/Z_2 > 0.4$) collisions, Kobal *et al.* [71,72] came to similar conclusions. With the calculated outer-shell ionization probabilities under 0.3 [44,66,69] for our more asymmetric ($Z_1/Z_2 \leqslant 0.1$) collisions, these post-collision rearrangements decrease the electron population of the *M* shell by only a few percent (see Fig. 8 in Ref. [53]). This would have changed the MI factors, which we calculate without an account for cascading electrons (see Tables V and VI), by no more than 1%. Moreover, as discussed in [69], the uncertain changes in the fluorescence and Coster-Kronig yields in solid targets [73–75] plus the complexity of the decay scheme for *L*-shell transitions and the lack of self-consistency in the selected database for such transitions [76] would make quantitative studies of the role of post collision rearrangement in *K*-shell ionization in the context of the *L*-subshell ionization highly unrealiable. Horvat *et al.* [53] found—and Kobal [72] confirmed this at low levels of *L*-shell ionization—that the effective *K*-shell fluorescence yield is insensitive to the assumed transition rates. Similarly, Lorenz and Hartmann [77] showed that the average changes in the *L*-shell fluorescence due to the original *L*-shell vacancy spectator are more reliable than the nuances of the transition probabilities for particular cascade schemes.

In the following figures 5–7, the ionization data extracted from our x-ray production measurements using the methods of [44,61] and [66,69] are plotted, respectively, as stars and triangles. The square symbols represent the data for ionization of Ce and Nd as reported by Braziewicz *et al.* [78].

IV. COMPARISON OF THE EXTRACTED *L*-SUBSHELL IONIZATION CROSS SECTIONS WITH THEORIES

In Fig. 5 our data and those of Braziewicz *et al.* [78] are compared with the predictions of the first Born, which is the sum of the PWBA [5] and OBKN [8] ionization cross sections, the ECPSSR [9,10], the ECUSAR [13], and the ECUSAR-IS which is the ECUSAR corrected for the IS effect. Due to simplifying assumptions, the coupled-state calculations of Sarkadi and Mukoyama [15–20] had underestimated subshell cross sections so that their sum was less than the total *L*-shell ionization cross section without the IS effect. Pajek *et al.* [13] rectified this problem by normalizing IS factors such that they merely redistributed collisionally

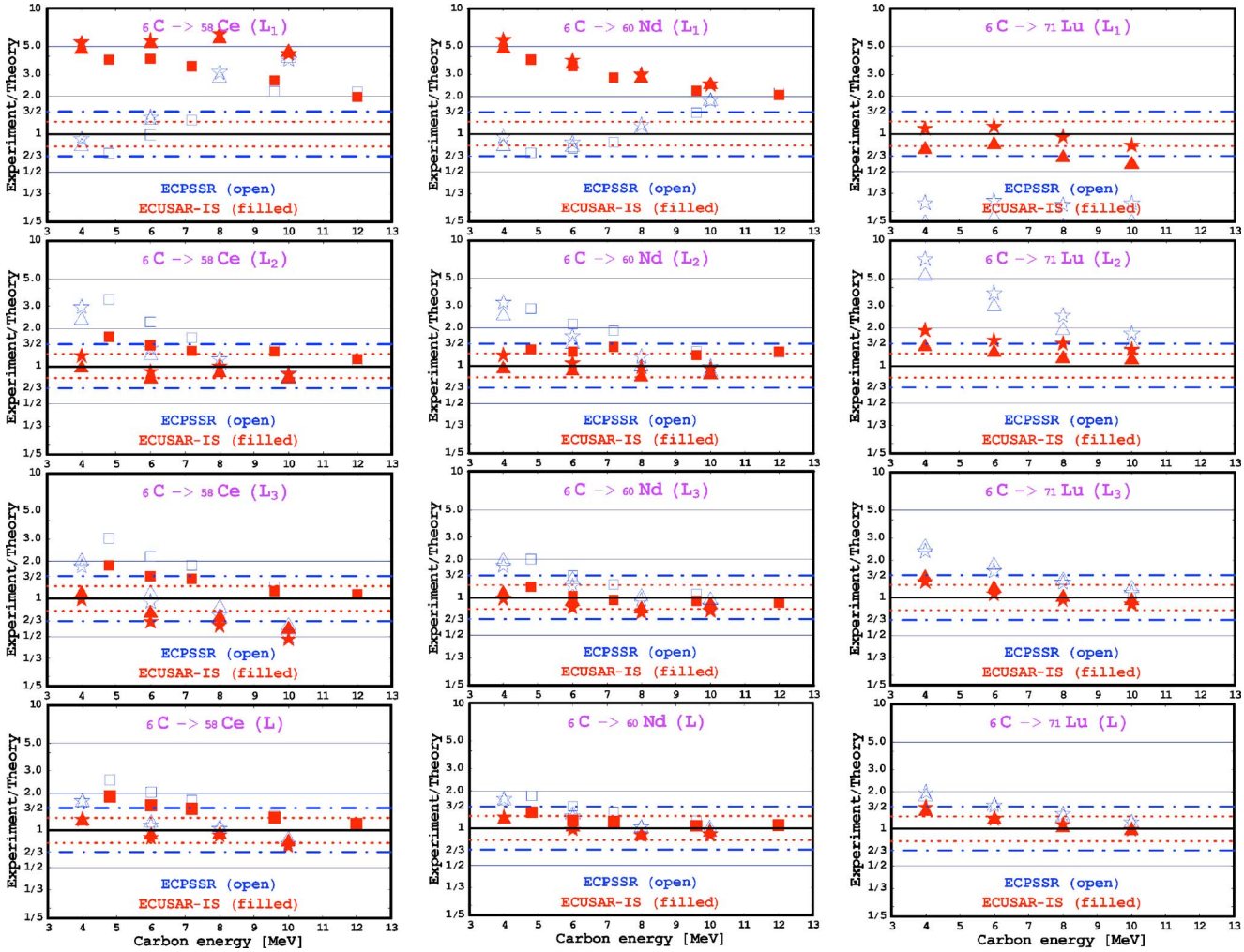

FIG. 6. (Color online) Ratios of the L_1, L_2, L_3, L-shell ionization cross sections for Ce and Nd from Ref. [78] (squares) and of the data extracted for our x-ray production measurements for Ce, Nd, and Lu according to Refs. [44,61] (stars) and Refs. [66,69] (triangles) to the predictions of the ECPSSR [9,10] (open symbols) and ECUSAR-IS [see Eq. (13)] (solid symbols) theories.

induced L-subshell vacancies without affecting the total L-shell cross section. We have normalized the IS factors c_i calculated according Sarkadi [79] so that $\Sigma\sigma_{L_i}^{\text{ECUSAR-IS}} = \Sigma\sigma_{L_i}^{\text{ECUSAR}}$. Hence

$$\sigma_{L_i}^{\text{ECUSAR-IS}} = c_i \cdot \sigma_{L_i}^{\text{ECUSAR}} \sum \sigma_{L_i}^{\text{ECUSAR}} \Big/ \sum c_i \cdot \sigma_{L_i}^{\text{ECUSAR}}. \tag{13}$$

As seen in Fig. 5—and amplified in Fig. 6, which exhibits a direct comparison of the ECPSSR and ECUSAR-IS theories as the ratio of the extracted ionization cross sections to the predictions of these theories—the ionization cross sections extracted for the L_1 subshell are the most difficult to predict. While the ECPSSR and ECUSAR-IS theories give reasonable agreement at lower carbon energies, at higher energies for $_{58}$Ce and $_{60}$Nd the extracted ionization data as well as those from Ref. [78] inexplicably tend to follow the first Born curve. Although these cross sections trace the shape of the curve calculated by the ECUSAR-IS theory, they systematically and substantially fall above that curve. This is consistent with what was observed before by Braziewicz *et al.* [78] for six other lanthanides with $57 \leqslant Z_2 \leqslant 68$ as well as with findings of others in ionization by carbon ions of heavier elements such as $_{70}$Yb and $_{79}$Au at 7–36 MeV [80], $_{72}$Hf, $_{73}$Ta, $_{74}$W, $_{76}$Os, $_{77}$Ir, $_{78}$Pt, $_{79}$Au, $_{83}$Bi, $_{90}$Th at 5.6–22.4 MeV [51], and $_{75}$Re, $_{78}$Pt, $_{79}$Au at 4–8 MeV [69]. On the other hand for $_{71}$Lu, our L_1 ionization data are within 20%, which is surprising in view of the large gap observed now in Ce and Nd and seen in other elements [51,69,78,80]. Yet, as illustrated in Ref. [69], the L_1 ionization cross section for $_{79}$Au bombarded by 2.5–3.4-MeV carbon ions [81] cross over from the ECPSSR curve at the highest energy to the ECUSAR-IS at the lowest energy. Moreover, our earlier gold data at 3.6–9.5 MeV [21]—contrary to our original conclusion based on the ECPSSR-IS with unnormalized IS factors [21]—are also in superb agreement with the ECUSAR-IS once the IS effect is normalized according to Eq. (13) (see Fig. 4 in Ref. [69]).

As demonstrated in Fig. 6, the ECUSAR-IS theory gives, with the exception of the 4-MeV point, similarly good agreement for the L_2 ionization of $_{71}$Lu and excellent agreement for $_{58}$Ce and $_{60}$Nd, while the measurements of Braziewicz *et al.* [78] for these elements are underestimated by as much as

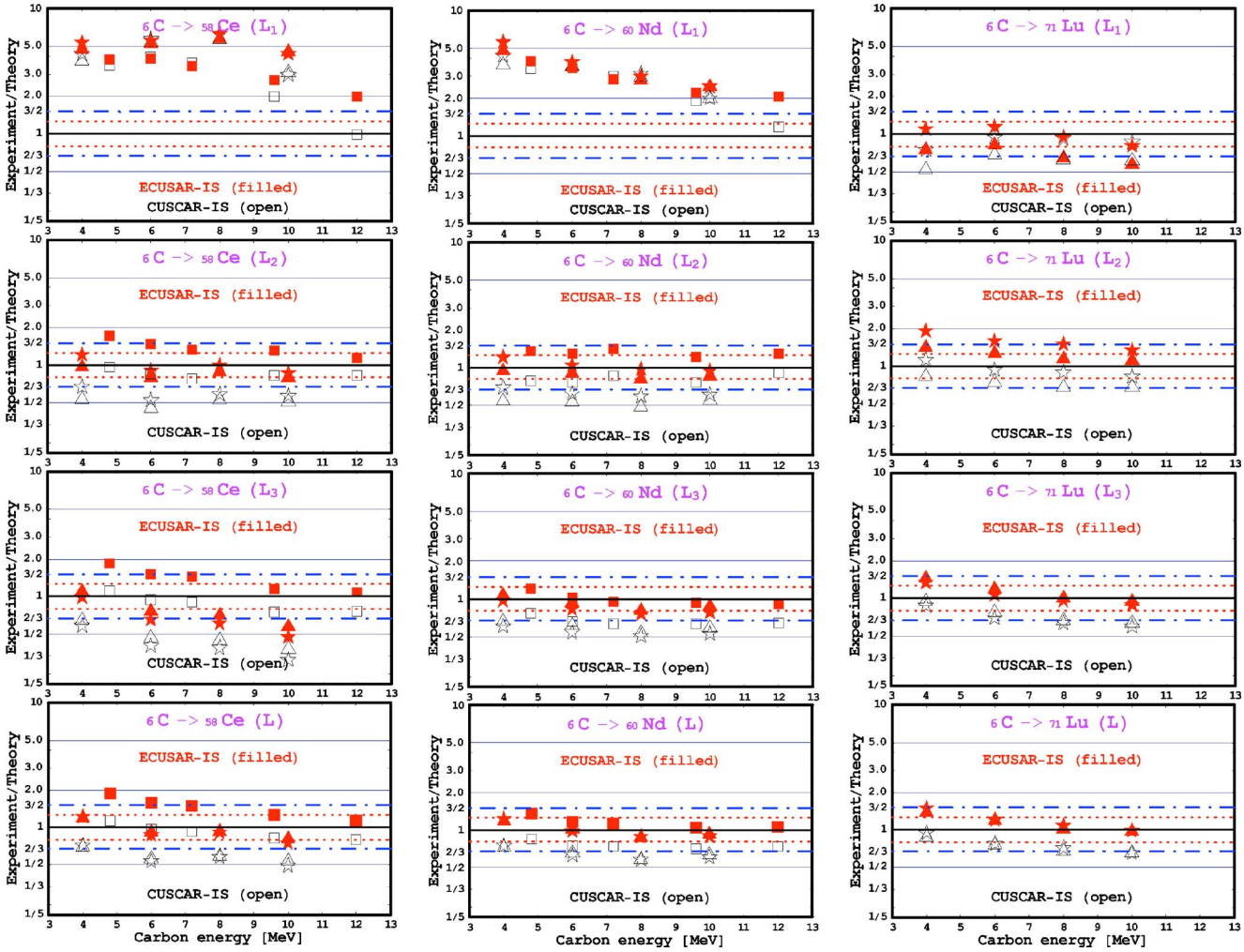

FIG. 7. (Color online) Ratios of the L_1, L_2, L_3, L-shell ionization cross sections for Ce and Nd from Ref. [78] (squares) and of the data extracted for our x-ray production measurements for Ce, Nd, and Lu according to Refs. [44,61] (stars) and Refs. [66,69] (triangles) to the predictions of the CUSCAR-IS [13] (open symbols) and ECUSAR-IS [see Eq. (13)] (solid symbols) theories.

70% for $_{58}$Ce at 4.8 MeV. This underestimation of the data from Ref. [74] rises to a factor of 2 in the ionization of the L_3 subshell of $_{58}$Ce at the lowest energy and disappears at the highest energy, while our data are in perfect agreement at the lowest energy, but are overestimated by a factor of 2 at the highest energy. For $_{60}$Nd, both Braziewicz *et al.* [78] and our data are in excellent (i.e., within 20%) agreement with the ECUSAR-IS theory of the L_3-subshell ionization as well as the total L-shell ionization that is dominated by the L_3 contribution. The same is true for our L_3 and L ionization of $_{71}$Lu with exception of the lowest energies where ECUSAR-IS theory underestimates the data by 40%.

Figure 7 contrasts the ECUSAR-IS and CUSCAR-IS, which is the semiclassical calculation of Trautmann *et al.* corrected for the normalized IS effect in the same manner as the ECUSAR. While the CUSCAR-IS cross sections are as much as a factor of 2 above the ECUSAR-IS at high 12 MeV, they converge to the L_1 subshell of Ce and Nd ionization data from Ref. [78] at this energy (see squares in Fig. 7). Based on our L_1-subshell measurements in Ce and Nd, the CUSCAR-IS is somewhat better than the ECUSAR-IS, although both theories underestimate the data at 10 MeV by a factor of 2 which telescopes to a factor 5 at 4 MeV. For L_2 and L_3 ionization at low energies, the CUSCAR-IS cross sections are almost a factor of 2 above the ECUSAR-IS, which brings them into accordance with the low-energy Ce measurements of Ref. [78] (see squares in Fig. 7). Based on our L_2 and L_3 data (see stars and triangles in Fig. 7), however, with the exception of Lu ionization by 4-MeV carbon ions the CUSCAR-IS overestimates them by as much as a factor of 2 while the ECUSAR-IS stays within 30% of all data except a factor of 2 underestimate of the Lu datum at 4 MeV.

V. CONCLUSIONS

The following are the main outcomes of the present investigation.

(1) The weighted average of L_i-subshell ionization cross sections extracted from two combinations of the measured x-ray production cross sections, $\{L\alpha, L\gamma_{1+5}, L\gamma_{2+3}\}$ and $\{L\alpha, L\gamma_{1+5}, L\gamma\}$, is (within a few percent) identical with L_i-subshell ionization cross section extracted only from $\{L\alpha, L\gamma_{1+5}, L\gamma_{2+3}\}$ measurements.

(2) A revision of the Datz technique for isolation of the $L\gamma_{2+3}$ x-ray production cross section is made. It relies on the $L\gamma_{1+5}$ rather than the $L\gamma_1$ cross section, multiplies $L\gamma_{4+4'}/L\gamma_{1+5}$ by $S\gamma_{2+3}/S\gamma_{4+4'}$—a factor which does depend on projectile energy due to multiple-hole ionization—and incorporates uncertainties of $L\gamma_{4+4'}/L\gamma_{1+5}$ in the fitting procedure. For the investigated collision system this revision results in small changes in the extracted L_i-subshell ionization cross sections relative to the outcome of the standard Datz technique [33]. It is expected that such a revision should become important for collision systems with larger and more projectile-energy dependent effects of multiple ionization i.e., in the regime of more symmetric and slower collisions.

(3) Use of different sets of single-hole atomic parameters gave practically (within 10%) the same results for the extracted *L*-subshell ionization cross sections.

(4) While individual atomic parameters may be substantially changed due to multiple ionization by heavy ions, the cancellation of opposite changes for the fluorescence and nonradiative yields leads to the extracted *L*-subshell ionization cross sections that are within 10%–35% of the cross sections extracted with single-hole atomic parameters.

(5) Further changes in the fluorescence and nonradiative yields due to vacancy rearrangements in the aftermath of multiple ionization and prior to x-ray emissions are estimated to be under 1%.

(6) Relative to the ionization cross sections extracted with the single-hole atomic parameters, two methods of accounting for multiple ionization showed that the procedures prescribed in Refs. [44] and [61] gave—to within 35%—generally higher cross sections while the method of Refs. [66] and [69] resulted—to within 15%—in generally lower cross sections for the L_1 and L_2 subshells. For the L_3 subshell, the procedures of Refs. [44] and [61] and those of Refs. [66] and [69] yielded, respectively, 15% and 10% lower cross sections. For the total *L* shell, both methods gave virtually the same ionization cross sections, which were about 10% below what they would have been if these methods were not applied.

(7) Except for the extracted L_1-subshell ionization of lutetium which was in surprisingly excellent accord with the ECUSAR-IS theory, the ECPSSR and ECUSAR were in substantially better agreement with the data than the predictions of the ECUSAR-IS and CUSCAR-IS theories that underestimate our Ce and Nd data for L_1-subshell ionization by factors of 2–5 as the carbon ion energy decreases from 10 to 4 MeV. These findings also apply to the L_1-subshell ionization in many other elements by carbon ions as reported in Refs. [51,69,81]. For the 12-MeV measurement of Ref. [78], the CUSCAR-IS gave very good agreement while the ECPSSR, ECUSAR, and ECUSAR-IS underestimated this datum by a factor of 2. Yet, as shown in Ref. [69], for the L_1-subshell ionization of gold, the 2.5-MeV measurement of Ref. [49] and our earlier 3.6–8.5-MeV cross sections [21] are in perfect agreement with the ECUSAR-IS after the proper normalization of the IS factors. On the other hand, the factor of 2 gap seen when the gold data of Refs. [21 and 51] are extrapolated to 3.5 MeV is troublesome. While possible reasons for long-standing problems with the L_1 subshell were recently discussed [69], they remain unresolved and should continue to be the primary focus of further studies.

(8) For L_2-subshell ionization, the ECUSAR-IS provides a substantial (as much as a factor of 3 at 4 MeV) improvement over the ECPSSR and ECUSAR theories. For Ce and Nd, the ECUSAR-IS is in excellent (i.e., with a 20% margin) agreement with our data at all energies. This agreement remains excellent for the 10-MeV measurement on Lu and deteriorates to a 70% underestimate at 4 MeV. The CUSCAR-IS is in excellent agreement for this datum and overestimates the 10-MeV measurement on Lu by 50%. Except for the 12-MeV datum from Ref. [78] for Nd and Ce, the CUSCAR-IS overestimates the L_2-subshell ionization by as much as a factor of 2.

(9) For L_3-subshell ionization, the ECUSAR and ECUSAR-IS are an equal 20%–50% improvement over the ECPSSR theory. Except for a factor of 2 overestimate of the Ce measurement at 10 MeV and a 40% overestimate of the Lu datum at 4 MeV, the ECUSAR and ECUSAR-IS are in excellent agreement with all data. Except for an excellent agreement with the 4-MeV datum for Lu, the CUSCAR-IS overestimates the L_3-subshell ionization by 50% at 10 MeV in this element. For Nd and Ce, respectively, the CUSCAR-IS overestimates the measured L_3-subshell ionization by as much as factors of 2 and 3.

(10) For total *L*-shell ionization, the trends are similar as for L_3-subshell ionization while the maximum discrepancies with our data are reduced to 40% for the ECUSAR and ECUSAR-IS and a factor of 2 for the CUSCAR-IS.

Further studies, both theoretical and experimental, are needed to clarify these findings.

ACKNOWLEDGMENTS

We thank the staff of the pelletron accelerator at IOP, Bhubaneswar for their skillful operation of the machine, and P. K. Das and S. Chatterjee for their technical help.

[1] G. Lapicki, J. Phys. Chem. Ref. Data **18**, 111 (1989).
[2] H. Paul and J. Sacher, At. Data Nucl. Data Tables **42**, 105 (1989).
[3] R. S. Sokhi and D. Crumpton, At. Data Nucl. Data Tables **30**, 49 (1984).
[4] I. Orlic, C. H. Sow, and S. M. Tang, At. Data Nucl. Data Tables **56**, 159 (1994).
[5] E. Merzbacher and L. W. Lewis, in *Encyclopedia of Physics*, edited by S. Flügge (Springer, Berlin, 1958), Vol. 34, p. 166.
[6] J. D. Garcia, E. Gerjuoy, and J. E. Welker, Phys. Rev. **165**, 66 (1968).
[7] J. Bang and J. M. Hansteen, K. Dan. Vidensk. Selsk. Mat. Fys. Medd. **31**, 13 (1959).
[8] V. S. Nikolaev, Zh. Eksp. Teor. Fiz. **51**, 1263 (1966) [Sov.

Phys. JETP **24**, 847 (1967)].
[9] W. Brandt and G. Lapicki, Phys. Rev. A **23**, 1717 (1981).
[10] G. Lapicki and F. D. McDaniel, Phys. Rev. A **22**, 1896 (1980); **23**, 975 (1981).
[11] D. Trautmann, F. Rösel, and G. Baur, Nucl. Instrum. Methods Phys. Res. **214**, 21 (1983).
[12] G. Lapicki, Nucl. Instrum. Methods Phys. Res. B **189**, 8 (2002).
[13] M. Pajek, D. Banaś, J. Semaniak, J. Braziewicz, U. Majewska, S. Chojnacki, T. Czyżewski, I. Fijał, M. Jaskóła, A. Glombik, W. Kretcschmer, D. Trautmann, G. Lapicki, and T. Mukoyama, Phys. Rev. A **68**, 022705 (2003).
[14] D. D. Cohen, Nucl. Instrum. Methods Phys. Res. B **49**, 1 (1990).
[15] L. Sarkadi and T. Mukoyama, J. Phys. B **14**, L255 (1981).
[16] L. Sarkadi and T. Mukoyama, Nucl. Instrum. Methods Phys. Res. B **61**, 167 (1991).
[17] L. Sarkadi, J. Phys. B **19**, 2519 (1986).
[18] L. Sarkadi, J. Phys. B **20**, L559 (1987).
[19] L. Sarkadi and T. Mukoyama, Phys. Rev. A **37**, 4540 (1988).
[20] L. Sarkadi and T. Mukoyama, J. Phys. B **23**, 3849 (1990).
[21] D. Bhattacharya, M. Sarkar, M. B. Chatterjee, P. Sen, G. Kuri, D. P. Mahapatra, and G. Lapicki, Phys. Rev. A **49**, 4616 (1994).
[22] M. Sarkar, D. Bhattacharya, M. B. Chatterjee, P. Sen, G. Kuri, D. P. Mahapatra, and G. Lapicki, Nucl. Instrum. Methods Phys. Res. B **103**, 23 (1995).
[23] D. Mitra, M. Sarkar, D. Bhattacharya, P. Sen, and G. Lapicki, Nucl. Instrum. Methods Phys. Res. B **152**, 207 (1999).
[24] V. B. Zlokazov, Comput. Phys. Commun. **28**, 27 (1982).
[25] E. Huttel, W. Arnold, H. Baumgart, and G. Clausnitzer, Nucl. Instrum. Methods Phys. Res. B **12**, 193 (1985).
[26] T. Papp, J. Palinkas, L. Sarkadi, B. Schlenk, I. Török, and K. Kiss, Nucl. Instrum. Methods Phys. Res. B **4**, 311 (1984).
[27] M. J. Berger and J. H. Hubbell, XCOM: NBSIR 87-3597, NBS, Washington, DC, 1987; http://physics.nist.gov/PhysRefData/Xcom/Text/XCOM.html
[28] J. H. Hubbell, P. N. Trehan, N. Singh, B. Chand, D. Mehta, M. L. Garg, R. R. Garg, S. Singh, and S. Puri, J. Phys. Chem. Ref. Data **23**, 339 (1994).
[29] S. I. Salem, L. Panossian, and R. A. Krause, At. Data Nucl. Data Tables **14**, 91 (1974).
[30] W. Melhorn, Phys. Lett. **26A**, 166 (1968).
[31] W. Jitschin, R. Hippler, K. Finke, R. Schuch, and H. O. Lutz, J. Phys. B **16**, 4405 (1983).
[32] D. Mitra, M. Sarkar, D. Bhattacharya, M. B. Chatterjee, P. Sen, G. Kuri, D. P. Mahapatra, and G. Lapicki, Phys. Rev. A **53**, 2309 (1996).
[33] S. Datz, J. L. Duggan, L. C. Feldman, E. Laegsgaard, and J. U. Andersen, Phys. Rev. A **9**, 192 (1974).
[34] W. Jitschin, R. H. Hippler, R. Shanker, H. Kleinpoppen, R. Schuch, and H. O. Lutz, J. Phys. B **16**, 1417 (1983).
[35] D. D. Cohen, J. Phys. B **17**, 3913 (1984).
[36] Y. P. Singh, D. Mitra, L. C. Trebedi, and P. N. Tendon, Phys. Rev. A **63**, 012713 (2000).
[37] J. L. Campbell and J. X. Wang, At. Data Nucl. Data Tables **43**, 281 (1989).
[38] http://www.physics.unc.edu/~macd/genls.html
[39] M. O. Krause, J. Phys. Chem. Ref. Data **8**, 307 (1979).
[40] S. Puri, B. Chand, D. Mehta, M. L. Garg, N. Singh, and P. N. Trehan, At. Data Nucl. Data Tables **61**, 289 (1995).
[41] J. L. Campbell, At. Data Nucl. Data Tables **85**, 291 (2003).
[42] J. H. Scofield, At. Data Nucl. Data Tables **14**, 121 (1974).
[43] F. P. Larkins, J. Phys. B **4**, L29 (1971).
[44] B. Sulik, G. Hock, and D. Berényi, J. Phys. B **17**, 3239 (1984); I. Kádár, S. Ricz, V. A. Shchegolev, B. Sulik, D. Varga, J. Végh, D. Berényi, and G. Hock, *ibid.* **18**, 275 (1985); B. Sulik, I. Kadar, S. Ricz, D. Varga, J. Vegh, G. Hock, and D. Berenyi, Nucl. Instrum. Methods Phys. Res. B **28**, 509 (1987); B. Sulik and G. Hock, in *Proceedings of the 2nd Workshop on High-Energy Ion Atom Collisions, Debrecen, 1984*, edited by D. Berényi and G. Hock (Akadémiai Kiadó, Budapest, 1985), p. 183.
[45] B. Sulik, Y. Awaya, T. Kambra, Y. Kanai, and T. Mizagawa, RIKEN Accel. Prog. Rep. **21**, 78 (1987).
[46] G. Lapicki, in *Proceedings of the 3rd Workshop on High-Energy Ion Collisions, Debrecen, 1987*, edited by D. Berényi and G. Hock, Lecture Notes in Physics, Vol. 294 (Springer, Berlin, 1988), p. 64.
[47] A. Berinde, C. Ciortea, A. Enulescu, D. Fluerașu, G. Hock, I. Piticu, L. Sarkadi, B. Sulik, and V. Zoran, J. Phys. B **20**, L481 (1987).
[48] I. Kádár, S. Ricz, J. Végh, B. Sulik, D. Varga, and D. Berényi, Phys. Rev. A **41**, 3518 (1990).
[49] B. Sulik, I. Török, A. Agoston, and I. Kádár, Nucl. Instrum. Methods Phys. Res. B **56/57**, 45 (1991).
[50] D. Bhattacharya, G. Kuri, D. P. Mahaparta, M. B. Chatterjee, and P. Sen, Z. Phys. D: At., Mol. Clusters **28**, 123 (1993).
[51] J. Semaniak, J. Braziewicz, M. Pajek, T. Czyżewski, L. Głowacka, M. Jaskóła, M. Haller, R. Karaschnick, W. Kretschmer, Z. Halabuka, and D. Trautmann, Phys. Rev. A **52**, 1125 (1995).
[52] B. Sulik, K. Tökési, Y. Awaya, T. Kambara, and Y. Kanai, Nucl. Instrum. Methods Phys. Res. B **154**, 286 (1999).
[53] V. Horvat, R. L. Watson, and J. M. Blackadar, Nucl. Instrum. Methods Phys. Res. B **170**, 336 (2000).
[54] M. Kavčič, M. Budnar, A. Mühleisen, P. Pelicon, Ž. Šmit, M. Žitnik, D. Castella, D. Corminboeuf, J.-Cl. Dousse, J. Hoszkowska, P.-A. Raboud, and K. Tökési, Phys. Rev. A **61**, 052711 (2000).
[55] M. Pajek, D. Banaś, J. Braziewicz, U. Majewska, J. Semaniak, T. Czyżewski, M. Jaskóła, W. Kretschmer, T. Mukoyama, D. Trautmann, and G. Lapicki, in *Application of Accelerators in Research and Industry*, edited by J. L. Duggan and I. L. Morgan, AIP Conf. Proc. No. 475 (AIP, Woodbury, NY, 1999), p. 32.
[56] D. Banaś, J. Braziewicz, U. Majewska, M. Pajek, J. Semaniak, T. Czyżewski, M. Jaskóła, W. Kretschmer, T. Mukoyama, and D. Trautmann, J. Phys. B **33**, L793 (2000).
[57] D. Banaś, J. Braziewicz, A. Kubala-Kukuś, U. Majewska, M. Pajek, J. Semaniak, T. Czyżewski, M. Jaskóła, W. Kretschmer, and T. Mukoyama, Nucl. Instrum. Methods Phys. Res. B **164/165**, 344 (2000).
[58] D. Banaś, M. Pajek, J. Semaniak, J. Braziewicz, A. Kubala-Kukuś, U. Majewska, T. Czyżewski, M. Jaskóła, W. Kretschmer, T. Mukoyama, and D. Trautmann, Nucl. Instrum. Methods Phys. Res. B **195**, 233 (2002).
[59] D. Banaś, J. Braziewicz, M. Czarnota, I. Fijał, M. Jaskóła, A. Korman, W. Kretschmer, M. Pajek, and J. Semaniak, Nucl. Instrum. Methods Phys. Res. B **205**, 139 (2003).

[60] M. Kavčič, Phys. Rev. A **68**, 022713 (2003).
[61] D. Banaś, J. Braziewicz, M. Pajek, J. Semaniak, T. Czyżewski, I. Fijał, M. Jaskóła, W. Kretschmer, T. Mukoyama, and D. Trautmann, J. Phys. B **35**, 3421 (2002).
[62] J. H. McGuire and P. Richard, Phys. Rev. A **8**, 1374 (1973).
[63] R. L. Becker, A. L. Ford, and J. F. Reading, Nucl. Instrum. Methods Phys. Res. B **3**, 43 (1984).
[64] M. H. Chen, B. Crasemann, and H. Mark, At. Data Nucl. Data Tables **24**, 13 (1979).
[65] M. H. Chen, B. Crasemann, K. N. Huang, M. Aoyagi, and H. Mark, At. Data Nucl. Data Tables **19**, 97 (1977).
[66] G. Lapicki, R. Mehta, J. L. Duggan, P. M. Kocur, J. L. Price, and F. D. McDaniel, Phys. Rev. A **34**, 3813 (1986).
[67] J. J. Thomson, Philos. Mag. **23**, 449 (1912).
[68] R. Mehta, H. L. Sun, D. K. Marble, J. L. Duggan, F. D. McDaniel, and G. Lapicki, J. Phys. B **28**, 1187 (1995).
[69] G. Lapicki, G. A. V. R. Murty, G. J. N. Raju, B. S. Reddy, S. B. Reddy, and V. Vijayan, Phys. Rev. A **70**, 062718 (2004).
[70] M. Czarnota, M. Pajek, D. Banaś, D. Chmielewska, J. Rzadkiewicz, Z. Sujkowski, J.-Cl. Dousse, M. Berset, O. Mauron, Y.-P. Maillard, P.-A. Raboud, J. Hoszowska, M. Polasik, and K. Słabkowska, Nucl. Instrum. Methods Phys. Res. B **205**, 133 (2003).
[71] M. Kobal, M. Kavčič, M. Budnar, J.-Cl. Dousse, Y.-P. Maillard, O. Mauron, P.-A. Raboud, and K. Tökési, Phys. Rev. A **70**, 062720 (2004).
[72] M. Kobal, Nucl. Instrum. Methods Phys. Res. B **229**, 165 (2005).
[73] H. O. Lutz, J. Stein, S. Datz, and C. D. Moak, Phys. Rev. Lett. **28**, 8 (1972).
[74] S. L. Sorensen, S. J. Schaphorst, S. B. Whitfield, B. Crasemann, and R. Carr, Phys. Rev. A **44**, 350 (1991).
[75] C. O. Reinhold, D. G. Arbó, J. Bürgdorfer, B. Gervais, E. Lamour, D. Vernhet, and J. P. Rozet, J. Phys. B **33**, L111 (2000).
[76] A. El-Shemi, Y. Lofty, and G. Zschornack, J. Phys. B **30**, 237 (1997).
[77] M. Lorenz and E. Hartmann, J. Phys. B **20**, 6189 (1987).
[78] J. Braziewicz, J. Semaniak, T. Czyżewski, L. Głowacka, M. Jaskóła, M. Haller, R. Karschnick, W. Kretschmer, and D. Trautmann, J. Phys. B **27**, 1535 (1994).
[79] L. Sarkadi, J. Phys. B **19**, L755 (1986).
[80] N. B. Malhi and T. J. Gray, Phys. Rev. A **44**, 7199 (1991).
[81] L. Sarkadi and T. Mukoyama, J. Phys. B **13**, 2255 (1980).